PCCP

PAPER

Cite this: *Phys. Chem. Chem. Phys.*, 2016, **18**, 28458

Osmotic pressures of lysozyme solutions from gas-like to crystal states†

Coralie Pasquier,[ab] Sylvie Beaufils,[b] Antoine Bouchoux,[ac] Sophie Rigault,[a] Bernard Cabane,[d] Mikael Lund,[e] Valérie Lechevalier,[a] Cécile Le Floch-Fouéré,[a] Maryvonne Pasco,[a] Gilles Pabœuf,[b] Javier Pérez[f] and Stéphane Pezennec*[a]

Received 3rd June 2016,
Accepted 16th September 2016

DOI: 10.1039/c6cp03867k

www.rsc.org/pccp

We obtained osmotic pressure data of lysozyme solutions, describing their physical states over a wide concentration range, using osmotic stress for pressures between 0.05 bar and about 40 bar and volume fractions between 0.01 and 0.61. The osmotic pressure *vs.* volume fraction data consist of a dilute, gas-phase regime, a transition regime with a high-compressibility plateau, and a concentrated regime where the system is nearly incompressible. The first two regimes are shifted towards a higher protein volume fraction upon decreasing the strength or the range of electrostatic interactions. We describe this shift and the overall shape of the experimental data in these two regimes through a model accounting for a steric repulsion, a short-range van der Waals attraction and a screened electrostatic repulsion. The transition is caused by crystallization, as shown by small-angle X-ray scattering. We verified that our data points correspond to thermodynamic equilibria, and thus that they consist of the reference experimental counterpart of a thermodynamic equation of state.

1 Introduction

Knowledge about the interactions in very concentrated solutions of proteins, namely up to a few hundred grams per liter, is of high relevance in various fields, such as the living cell physiology, food transformation (foams, powders, membrane filtration…), pharmacology and drug delivery, or diseases implying the phase transition of proteins.[1–7] Predictive models, relying mostly on the knowledge gained from colloidal physics, have been proposed for the behavior of concentrated proteins.[8–10] However, they fail to determine the complexity and the variability of the protein molecules, related to the combination of their different levels of structures with the distinct physicochemical properties of amino acid residues.

Osmotic pressure measurements enable us to probe protein–protein, protein–ion or protein–solvent interactions. Data on globular proteins have been established in the past,[11–14] however the highest concentrations that were obtained were never high enough to enable the system to go out of a dilute or semi-dilute range. In this work we report results obtained through osmotic stress[15–23] as a concentration technique. This method makes it possible to control the osmotic pressure over a wide range of volume fractions (spanning from the dilute phase to phases where interactions play a prominent role, up to the solid phase) and to reach the same concentration state by different pathways, while keeping constant the salt activity.

We study lysozyme, a globular protein, that has been well characterized since its discovery in 1922. Numerous studies have been conducted on lysozyme, in particular its self-interaction characteristics when concentrated or subjected to changes in the physicochemical conditions.[9,24–35] Specifically, lysozyme has been shown, as other non-protein colloids, to exhibit a combination of long-range repulsive and short-range attractive interactions, which leads to the formation of equilibrium clusters.[24,25]

In the present work, we aim to bring answers to the following questions:

- Do the diagrams relating osmotic pressure Π to volume fraction ϕ enable us to identify transitions of the system when concentration is increased?
- If we tune the interactions, do the diagrams reflect the changes? Is it in a predictable way?

[a] *STLO, Agrocampus Ouest, INRA, 35000, Rennes, France. E-mail: stephane.pezennec@inra.fr*
[b] *Institut de Physique de Rennes, UMR6251 CNRS-Université de Rennes 1, F-35042 Rennes, France*
[c] *LISBP, UMR 5504/792 INRA-CNRS-INSA, 135 avenue de Rangueil, F-31077 Toulouse CEDEX 04, France*
[d] *Laboratoire CBI, CNRS UMR 8231, Université Pierre et Marie Curie, Université Diderot, ESPCI, 10 rue Vauquelin, F-75231, Paris CEDEX 05, France*
[e] *Department of Theoretical Chemistry, Lund University, P.O. Box 124, SE-22100 Lund, Sweden*
[f] *Synchrotron SOLEIL, F-91192 Gif-sur-Yvette, France*

† Electronic supplementary information (ESI) available: Net charge of lysozyme as a function of pH (Fig. S1); reversibility of osmotic stress at 150 mM and 35 mM ionic strengths (Fig. S2 and S3); Fourier transform infrared spectra and secondary structure of lysozyme, experimental procedure and results (Fig. S4); small-angle X-ray scattering, experimental procedure and results (Fig. S5); generalized van der Waals (GVDW) model; fitting of the GVDW model with and without screening of electrostatic interactions by counterions (Fig. S6); impact of the value of the radius of the lysozyme model on the osmotic pressure predicted by the GVDW model (Fig. S7); references. See DOI: 10.1039/c6cp03867k

• What are the positions of the (ϕ, Π) lines with respect to theoretical models for simple colloids?

• Are the (ϕ, Π) diagrams that we obtain for lysozyme the experimental reference for true equations of state (EOS)?

2 Materials and methods

Sample preparation

Lysozyme hydrochloride powder (lysozyme purity higher than 98%, as determined by reversed-phase high-performance liquid chromatography (HPLC)) was a gift from LIOT (Annezin, France). Stock solutions were prepared by solubilizing protein in 18 MΩ resistivity Milli-Q water (Merck Millipore, Darmstadt, Germany) and were kept at 4 °C.

Osmotic stress technique

The osmotic stress experiments were performed according to the procedure described by Bouchoux *et al.*[20] The osmotic stress technique is based on osmosis: the disequilibrium of chemical potentials between the interior of the dialysis bag, containing the protein solution, and the surrounding medium of controlled osmotic pressure causes a water flow from the high to the low chemical potential compartments. When the high chemical potential side is the protein solution, the latter is concentrated until equilibrium is reached.

We used four types of bis-tris propane–HCl buffers: pH 7 and 20 mM, 35 mM, and 150 mM ionic strength, and pH 9 and 20 mM ionic strength. Lysozyme net charges of +8.3 *e* and +6.3 *e* at pH 7 and pH 9, respectively, were predicted from its three-dimensional structure (PDB ID: 2VB1[36]) using PROPKA[37,38] (see also Fig. S1, ESI†). Each buffer contained 0.2 g L^{-1} of thimerosal (Sigma, Saint Louis, USA) in order to avoid bacterial development. The bis-tris propane total concentration was chosen to account for an ionic strength of 20 mM, depending on the pH: 11.3 mM at pH 7 and 40 mM at pH 9. Ionic strengths of 35 mM and 150 mM were obtained by adding NaCl. Thimerosal, bis-tris propane (1,3-bis[tris(hydroxymethyl)methylamino]propane) and NaCl were bought from Sigma-Aldrich (Saint-Louis, USA).

Polymer solutions were prepared directly in 500 mL glass bottles, by mixing the desired amount of polyethylene glycol (PEG) 20 000 (Sigma-Aldrich, Saint-Louis, USA) and buffer at 20 °C. To relate PEG 20 000 concentrations and osmotic pressures, we used the single-parameter phenomenological equation of state of PEG established by Cohen *et al.*,[39] assuming a prefactor $\alpha = 0.44$, a monomer mass $M_m = 44$ Da and a specific partial volume $\bar{V} = 0.825$ mL g^{-1} for PEG 20 000:

$$\Pi N^{9/5} = \frac{RT}{M_m \bar{V}}\left(\frac{C}{C_N^*} + \alpha\left(\frac{C}{C_N^*}\right)^{9/4}\right) \quad (1)$$

where N is the number of monomers per PEG molecule. The concentration C_N^* is defined by:

$$C_N^* = \frac{N^{-4/5}}{\bar{V}} \quad (2)$$

Polymer solutions were kept at 20 °C during the whole experiments.

We used a SpectraPor Dialysis Membrane, with a 6–8 kDa molecular mass cutoff and a 6.4 mm diameter (SpectrumLabs, Rancho Dominguez, USA) for the dialysis bags. Such a mass cutoff allows free exchange of ions and water, but not that of proteins and PEG 20 000. For each bag, a 10 cm length of dialysis membrane was cut and rinsed in Milli Q water. The bag was then filled with a protein stock solution of low concentration (50 g L^{-1} for osmotic pressures higher than 0.39 bar, and 10 g L^{-1} for pressures of 0.05 bar and 0.12 bar) and immersed in the polymer solution.

Due to the water efflux, the volume of the dialysis bags decreased. Dialysis bags were frequently taken out of the polymer solution, rinsed carefully with deionized water in order to avoid contamination of the protein solution with PEG 20 000, then opened and re-filled with the low-concentration protein solution. The already stressed, concentrated solution and the new, dilute one were then homogenized, and the bag was put back in the polymer solution.

As the increase in the concentration of the solution inside the bags can be very important, especially for solutions subject to high osmotic pressures, the solutions subject to pressures higher than 1.16 bar were first equilibrated to 1.16 bar for one week. The solutions subject to pressures lower than 1.16 bar were directly put to their final osmotic pressure. After one week, all the bags were transferred into new polymer solutions, of their final osmotic pressure. They were kept in these solutions for two weeks, during which they were frequently re-filled, in order to obtain a weight of protein solution that was sufficient to make a dry content analysis (more than 1 g). At the end of the two weeks, the bags were considered of sufficient volume and were no more re-filled. However, during the two weeks, some water flowed out of the bags and diluted the polymer solution, which decreased slightly the external osmotic pressure. Thus, the bags were finally transferred into new polymer solutions of the desired osmotic pressure, and kept without re-filling for one more week. At the end of these four weeks, the protein solution was considered to be in equilibrium with the surrounding polymer solution.

For decompression experiments, the protein solution was first equilibrated at the desired final osmotic pressure following the procedure described above. Then, the dialysis bag was put in a polymer solution of higher osmotic pressure for a week, without re-filling it. Finally, the bag was put back in a polymer solution inducing the same osmotic pressure as that applied initially. In the following, we shall refer to this compression–decompression cycle as ''two-way compression''.

Dry content measurement

This technique was used to determine the concentration of protein in the concentrated solutions obtained using osmotic pressure.

We used stainless steel cupels (diameter 60 mm, height 25 mm), with a removable lid. In each cupel, we put 25 g of Fontainebleau sand. The cupels and small glass rods were kept in an oven at 102 °C for a minimum period of 2 h, with the lid open, in order to eliminate remaining water. The cupels and

rods were then left to cool at room temperature in a dessicator containing recently dehydrated silica gel, under vacuum, for a minimum period of 45 min.

After cooling, each cupel was weighed (precision of 0.1 mg) with its lid closed and a glass rod. Each bag was rinsed, and then opened and the protein solution was quickly put in a cupel. The total (cupel, lid, sample and glass rod) was then weighed. The sample was mixed with the Fontainebleau sand with the glass rod, which was left inside the cupel. The cupel (lid open) was then put in an oven at 102 °C overnight.

The day after, each cupel with its glass rod (lid closed) was left to cool at room temperature in a dessicator containing recently dehydrated silica gel for minimum 45 min. After cooling, each cupel was weighed (precision of 0.1 mg) with its lid closed.

Dry content weights were corrected for sodium chloride and bis-tris propane weights. Conversion from weights to volume fractions was performed considering that lysozyme had a specific partial volume of 0.712 mL g^{-1}.[40]

Dynamic vapor sorption (DVS)

Desorption isotherms of a 50 g L^{-1} lysozyme solution were obtained using a dynamic vapor sorption analyzer DVS (Surface Measurement Systems Ltd, London, UK) equipped with a Cahn microbalance. The experiments were carried out at constant temperature (20 °C) and relative humidity values of 5%, 60% and 90%, to reach water activity values of 0.05 and 0.6 and 0.9, respectively, at the equilibrium.

The water activity was converted to osmotic pressure using the formula:

$$\Pi = -\frac{RT}{v_a}\ln(a_w) \quad (3)$$

with Π being the osmotic pressure (in Pa), R the universal gas constant, T the temperature, v_a the molar volume of water and a_w the water activity.

3 Results

3.1 Osmotic pressure profiles of lysozyme in a pH 7, I = 20 mM buffer

Fig. 1 presents the measured values of the protein volume fraction (horizontal axis) according to the osmotic pressures applied to the solution of lysozyme in a buffer at pH 7 and ionic strength 20 mM. Under these conditions the net charge per protein is +8.3 e (see Materials and methods). For comparison, we plotted the van't Hoff law of ideal gases, $\Pi = \rho k_B T$, where ρ is the number density and k_B the Boltzmann constant, and the Carnahan–Starling EOS[41] $\Pi = \rho k_B T \frac{1+\phi+\phi^2-\phi^3}{(1-\phi)^3}$, where ϕ is the volume fraction, which describes a hard sphere gas,[15] using the lysozyme molecular weight (14 313 Da)[42] and the partial specific volume (0.712 mL g^{-1})[40] so that the volume and the mass of the equivalent spheres are equal to those of the proteins. The radius of the equivalent spheres is 1.59 nm.

The data demonstrate that osmotic stress makes it possible to cover three decades in osmotic pressures and two decades in volume fractions. At very high pressures, our data for pH 7 and ionic strength 35 mM match the results obtained by Rickard *et al.* through single particle sorption[29] and our own dynamic vapor sorption (DVS) results. It is noteworthy that, in contrast to osmotic stress, DVS and Rickard's microparticle technique concentrate all solutes, including salts, so that the ionic strength may vary.

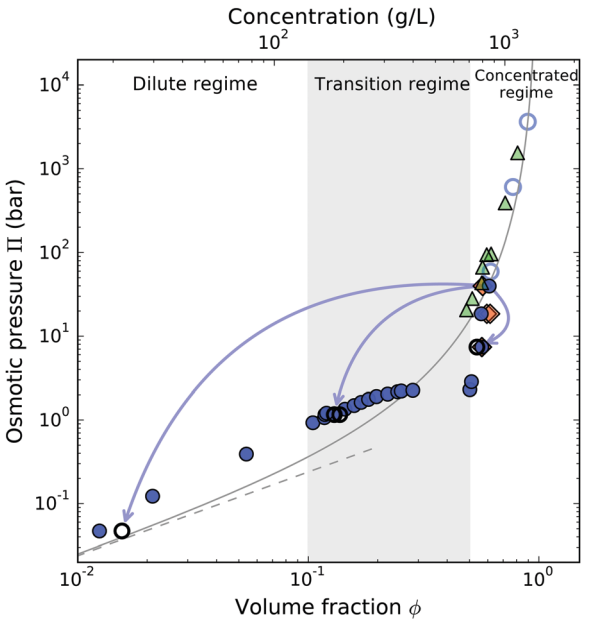

Fig. 1 (ϕ, Π) diagram of lysozyme in a pH 7, I = 20 mM bis-tris propane buffer, obtained by one-way compression (filled blue circles), or by compression to 39.75 bar followed by decompression to different pressures ("two-way compression", empty black circles): the arrows symbolize the decompression part of the two-way compression experiments. The solid line represents the Carnahan–Starling model and the dashed black line represents the van't Hoff model. Data from the study of Rickard *et al.*[29] obtained by bulk vapor desorption are represented by green triangles. Our data from dynamic vapor sorption (DVS, empty blue circles) were obtained using lysozyme solutions initially at pH 7 and 35 mM ionic strength, but DVS does not keep concentrations constant. Crystal densities extracted from SAXS data (see discussion, Section 4.2) are represented by orange diamonds.

The osmotic pressure profile can be divided into three parts: a dilute regime, up to ϕ = 0.1; a transition regime, ranging from ϕ = 0.1 to 0.5, where the slope of the curve decreases until a plateau, characterized experimentally by a large step in volume fraction (almost two-fold increase); then a concentrated regime, above ϕ = 0.5, where the pressure increases steeply with volume fraction.

The use of the van't Hoff and Carnahan–Starling models is generally restricted to fluid, dilute systems.[43] In our case, in the dilute regime, the pressures of the lysozyme solutions are approximately twice as large as the Carnahan–Starling model or a van't Hoff perfect gas system. In the discussion, Section 4, we shall present a model that explains the origin of this excess pressure.

3.2 Morphology of lysozyme solutions in a pH 7, I = 20 mM buffer

The pictures shown in Fig. 2 have been chosen to illustrate the changes in the morphology of the lysozyme solution (pH 7, I = 20 mM buffer) subjected to different osmotic pressures.

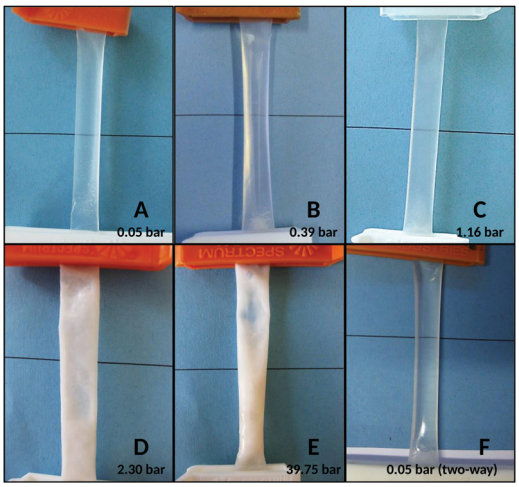

Fig. 2 Photographs of dialysis bags containing lysozyme at pH 7 and 20 mM ionic strength, subjected to different osmotic pressures: 0.05 bar (A), 0.39 bar (B), 1.16 bar (C), 2.30 bar (D) and 39.75 bar (E). Photograph (F) shows the bag after compressing the solution from 0.05 to 39.75 bar, and then decompressing it back to 0.05 bar.

The 10 g L^{-1} and 50 g L^{-1} (ϕ = 0.0071 and 0.0356, respectively) stock solutions are clear, transparent liquids that flow easily. Samples obtained by osmotic compression have the same aspect as the stock solutions from 0.05 bar (Fig. 2A) to 0.12 bar. When the solutions are concentrated further, they become increasingly dense but remain transparent, with some white, fluffy aggregates visible at the bottom of the bag (Fig. 2B and C). For pressures above 2.26 bar, namely above the "large volume fraction step" (see Section 3.1), the samples become white and solid (Fig. 2D and E). If a sample is compressed to 0.05 bar, then 39.75 bar, and finally de-compressed to 0.05 bar without any mechanical treatment, the solid re-dissolves spontaneously and completely, and becomes as clear and liquid as the original sample compressed at 0.05 bar, without any insoluble part remaining (Fig. 2F). This morphological reversibility needs to be confirmed from a thermodynamic point of view, as addressed in the following section.

3.3 Thermodynamic reversibility of the compression

We designed several experiments in order to verify that the same points on the osmotic pressure profile can be attained through different paths.

We performed osmotic compressions at 0.05 bar, 1.16 bar and 7.40 bar at pH 7 and I = 20 mM. After equilibrium was reached, we immersed the dialysis bags in a PEG solution at a 39.75 bar osmotic pressure. After a new equilibrium, we brought each bag back to its initial osmotic pressure ("two-way compression").

As shown in Fig. 1, for 3 cycles with different final osmotic pressures, we found that the final volume fractions were similar for samples obtained through one-way compression and through two-way compression.

We performed additional experiments at pH 7, I = 35 mM and pH 7, I = 150 mM (see Fig. S2 and S3, ESI†), and we also changed the pathways of the cycles: for pH 7 and I = 35 mM (Fig. S3, ESI†), each sample was compressed to a different osmotic pressure and were then decompressed to the same osmotic pressure (0.57 bar). The results confirm that, on both sides of the "large volume fraction step", one-way and two-way compressions are equivalent.

3.4 Influence of pH and ionic strength

In another set of osmotic stress experiments, we reduced the net charge of the protein to Z = +6.3 e (see Materials and methods) by using a pH 9, I = 20 mM bis-tris propane buffer. Alternatively, we kept pH at 7 but adjusted the ionic strength to 35 mM and 150 mM by adding NaCl. Fig. 3 presents the (ϕ, Π) diagrams obtained for each condition, compared with the (ϕ, Π) diagram obtained at pH 7, I = 20 mM.

Increasing pH at constant ionic strength or increasing the ionic strength at constant pH causes a shift in the experimental curve towards lower osmotic pressures in the dilute and the transition regimes. However, in the concentrated regime, the volume fraction is the same for all the conditions. Whatever pH and ionic strength, the evolution of the solution morphology follows the same pattern as for pH 7, I = 20 mM, showing in particular solidification for concentrations above the "large volume fraction step".

4 Discussion

The results presented above demonstrate that the use of osmotic stress applied through a dialysis equilibrium makes

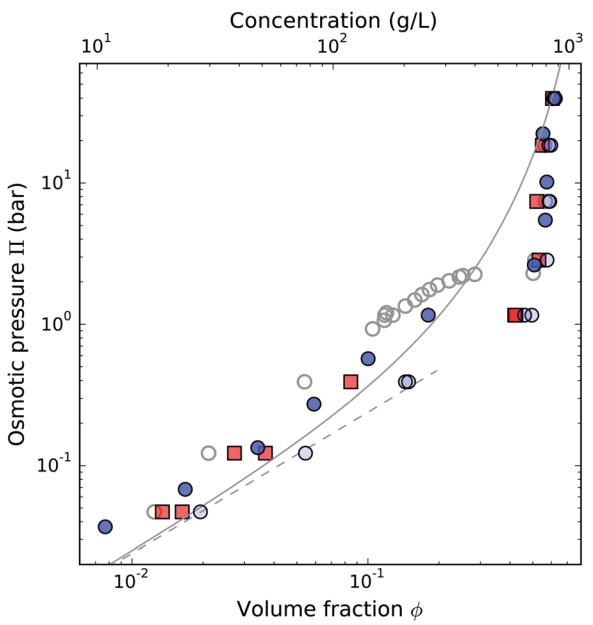

Fig. 3 (ϕ, Π) diagrams of lysozyme for several physicochemical conditions. Conditions presented are: pH 7, ionic strength I = 20 mM (grey empty circles); pH 7, I = 35 mM (dark blue circles); pH 7, I = 150 mM (light blue circles) and pH 9, I = 20 mM (red squares). The solid line represents the Carnahan–Starling model and the dashed line represents the van't Hoff model.

it possible to cover a volume fraction/osmotic pressure range that joins, at high concentrations, the data obtained through vapor sorption[29] (Fig. 1). The lowest concentrations that we have studied match the lysozyme concentration in egg white and the highest ones reach those commonly met in industrial processes.

The first aim of this section is to show that the reported (ϕ, Π) diagrams, unambiguously relating the volume fraction to the osmotic pressure of lysozyme solutions under chosen ionic conditions, consist of the reference experimental counterpart of equations of state (EOS) for lysozyme solutions. We shall then address the nature of the transition regime and its relationship to the volume fractions of the concentrated regime, by considering the nature of the interactions between solutes under the ionic conditions that are imposed by the outer stressing solution.

4.1 The (ϕ, Π) diagrams are reference experimental data for equations of state

The first argument comes from the thermodynamic reversibility of the transformations of the system. Preliminary observations of the morphology gave us a clue about this reversibility, as the samples get back to their liquid, clear form when decompressed to low osmotic pressures, even after having been strongly compressed at 39.75 bar. Focusing on the (ϕ, Π) diagrams reveals that compressing a lysozyme solution to 39.75 bar and decompressing it back to a lower pressure is equivalent to a one-way compression to the lowest pressure, for ionic strengths ranging from 20 mM to 150 mM at pH 7. The analysis of the pH 7, I = 20 mM samples by Fourier transform infrared spectroscopy (FTIR) clearly showed that the system was composed of the same structural entities, regardless of the volume fraction or the pathway (Fig. S4, ESI†). All these features proved that the state of the solution reversibly depends on the pressure, volume fraction and physicochemical conditions, and not on the compression history.

Considering the above discussion, in addition to the fact that the diagrams originate from several datasets and batches of protein, we can state that we established the reference experimental data for equations of state (EOS) of lysozyme solutions, for ionic strengths up to 150 mM.

4.2 Nature of the transition regime

Since our data points identify equilibrium states of the system, the existence of a plateau, where the chemical potential of water remains nearly constant over a large range of volume fractions, must reflect the existence of a phase transition.

Small angle X-ray scattering (SAXS) data obtained in the concentrated regime reveal lysozyme crystallization, as shown by Bragg peaks, under all ionic conditions up to I = 150 mM. As an example, the structure factors of lysozyme solutions in a pH 7, I = 20 mM buffer compressed at 1.16 bar and 39.75 bar are presented in Fig. S5, ESI.† We therefore propose that the phase transition evidenced by the (ϕ, Π) diagrams is caused by crystallization of the protein. This hypothesis is consistent with the solubilities determined by Retailleau *et al.*[44] for lysozyme at pH 6.5 and different NaCl concentrations (ϕ = 0.25, 0.15 and 0.10 for 0 mM, 50 mM and 100 mM NaCl, respectively).

We interpret the SAXS spectra as powder diffraction spectra. The major crystalline form is tetragonal, of the $P4_32_12$ space group, as found in numerous crystallographic structures of lysozyme (see *e.g.* 1HEL[45]). Fitting the lattice parameters allows us to estimate the volume fraction of protein in the crystal. As shown in Fig. 1, the values that result from the fit are quite consistent with the volume fractions of the samples in the concentrated regime, indicating that all the lysozyme was crystallized in these samples. The volume fraction variations between the points shown in the diagram are related to slight changes in the $P4_32_12$ lattice parameters.

Rickard *et al.*[29] found higher osmotic pressures at volume fraction ϕ = 0.52 and did not mention crystallization. This is easily explained by the kinetics of concentration in that case. Indeed, the dehydration method used by Rickard *et al.* causes a rapid concentration of the lysozyme solution, leading to a glassy state within the compressed droplets. Therefore the crystals do not nucleate, and the (ϕ, Π) diagram follows a liquid-like tendency, parallel to the Carnahan–Starling model, instead of following the bend caused by crystallization in our slow equilibrium experiments. The ratio of osmotic pressures of the glassy and crystal states ($\times$10) is comparable with the solubility ratios commonly found for amorphous and crystalline solids.

The question then arises from the smoothness of the change in the slope at the beginning of the transition regime. Indeed, as soon as the nuclei of the crystal have reached the critical size, crystallization should occur without any barrier. Therefore the concentration in the liquid protein phase would remain constant as the chemical potential of lysozyme must be the same in the liquid and crystallized phases. Accordingly, the data would then show an angular profile at the leading edge of the plateau, instead of the smooth pretransition bending shown in Fig. 1 and 3.

The existence of an intermediate regime of sub-critical nuclei, or equilibrium clusters,[24,25] could explain the pre-transition bending, as the concentration range where the equilibrium clusters have been observed (ϕ = 0.12–0.23) is consistent with most of the transition regime of the (ϕ, Π) diagram, and the conditions are quite close to ours:[25] low ionic strength, pH 7.8 instead of 7, and the same temperature, 25 °C. In the next section, we will however show that the pre-transitional bending can also be explained quantitatively by the effects of ionic screening and van der Waals forces.

4.3 Interactions between proteins

Since the structure of lysozyme molecules remains the same through the whole range of pressures and volume fractions, it becomes interesting to compare the osmotic pressures of their solutions with those from dispersions of monodisperse spherical particles. A first observation is that the Carnahan–Starling equation of state provides a surprisingly good fit to the data over 4 decades in pressures, and even at concentrations where the virial equation of state with only 2-body interactions is not expected to hold (Fig. 1). Here we show that deviations

from the Carnahan–Starling equation can be partly accounted for by taking into account the ionic interactions between proteins, and their interactions due to van der Waals forces.

To explain the impact of ionic conditions on osmotic pressures in the dilute regime, with the simple hypotheses that lysozyme molecules are spheres with a uniform surface charge density and following a mean-field approach, we developed a generalized van der Waals (GVDW) model (see the full development in the ESI†) leading to the expression of the osmotic pressure as a function of an effective pair potential:

$$\beta\Pi\frac{v}{\phi} = \frac{1+\phi+\phi^2-\phi^3}{(1-\phi)^3} + 2\pi\frac{\phi}{v}\int_{2a}^{\infty}\beta w(r)r^2\mathrm{d}r \qquad (4)$$

where $\beta = 1/k_BT$ is the reciprocal of the thermal energy, Π is the osmotic pressure, v is the protein molecular volume, ϕ is the volume fraction, a is the molecular hard-core radius, r is the intermolecular center-to-center distance and w is an effective pair potential.

In order to account for the shift of the experimental osmotic pressures upon changes in pH or ionic strength, we describe the contribution of screened ionic repulsions to the pair potential by a Debye–Hückel potential

$$\beta w_{DH}(r) = \frac{Z^2 L_B}{(1+\kappa a)^2}\frac{e^{-\kappa(r-2a)}}{r} \qquad (5)$$

where Z is the molecular charge and L_B is the Bjerrum length. κ is the reciprocal of the screening length and, if the protein counterions are taken into account, κ is defined by:

$$\kappa^2 = 4\pi L_B N_A(2C_S + ZC_P) \qquad (6)$$

where N_A is the Avogadro constant, C_S is the pair concentration of monovalent salt and C_P is the protein molar concentration.

The contribution of short-ranged van der Waals forces to the effective pair potential is accounted for by a Hamaker potential

$$\beta w_H(r) = -\frac{A_H}{6}\left(\frac{2a^2}{r^2-4a^2} + \frac{2a^2}{r^2} + \ln\left(\frac{r^2-4a^2}{r^2}\right)\right) \qquad (7)$$

for $r > 2a$, infinity otherwise, where A_H is the Hamaker constant (in k_BT units).

The total pair potential can be written as $w(r) = w_{DH}(r) + w_H(r)$, and the expression of osmotic pressure given by eqn (4) can then be fitted to the experimental data, through numerical integration of its interaction term, using the Hamaker constant A_H as the only adjustable parameter (the lower integration limit was increased by 0.02 nm to avoid divergence).

We fit this model in the packing fraction region below the crystallization, with a global A_H, common to all pH and ionic strength conditions. The protein charge Z was fixed to the theoretical net charge of the protein for the considered pH. The results are shown in Fig. 4, where the model is drawn on the experimental points used for the fitting.

In spite of large approximations (lysozyme figured as a spherical molecule with uniform surface charge density, mean-field model assuming a step-shaped pair correlation function), our single-parameter GVDW model accounts strikingly well for the shape of the experimental data in the low-concentration range, as well as for their tendency to shift upon changes in the ionic conditions.

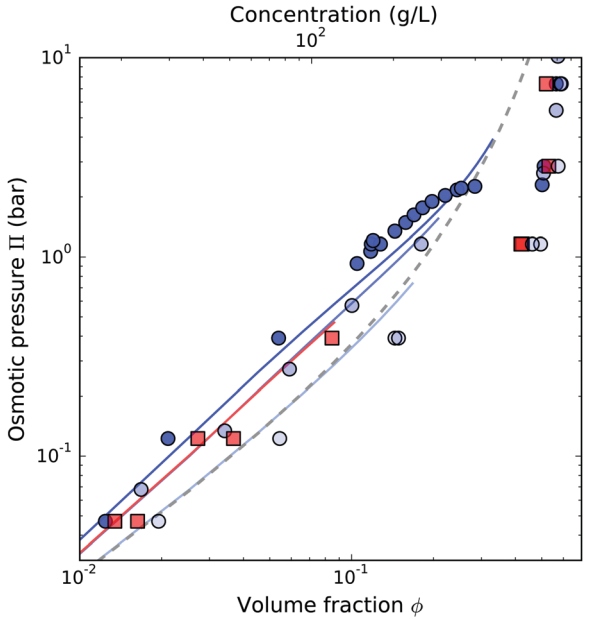

Fig. 4 Fit of the generalized van der Waals model to the experimental osmotic pressures of lysozyme in the dilute region. The model (solid lines) was fitted simultaneously to the 4 plotted series of experimental data, using Z/e values of 8.3 and 6.3 at pH 7 (circles) and pH 9 (squares), respectively. The corresponding fitted value of the Hamaker constant is 3.76 k_BT. Conditions are pH 7, I = 20 mM (dark blue), pH 7, I = 35 mM (medium blue), pH 7, I = 150 mM (light blue) and pH 9, I = 20 mM (red). The model lines are plotted only in the volume fraction range used for the fit. The dashed line represents the Carnahan–Starling model.

As regards the shape of the (ϕ, Π) diagrams, especially the downward bending observed below the crystallization plateau, it is important to point out that the counterions of the proteins strongly screen the electrostatic interactions, especially at high protein volume fractions, and that it is necessary to take this contribution into account in order to reproduce the shape of the data in the dilute and transition regime (see Fig. S6, ESI† for example at pH 7 and ionic strength 20 mM). The increase of the concentration of these counterions, and thus of the effective ionic strength, with volume fraction may be a cause of the existence of equilibrium clusters in a concentration range that is consistent with the transition regime of the (ϕ, Π) curve. Indeed, the bending of the curve occurs when the counterion concentration is sufficient to decrease significantly the repulsions between proteins and thus favors the attractions, giving rise to a new balance of interactions. Moreover, the aggregation number of the equilibrium clusters has been shown to be related to changes that favor attractions over repulsions, such as a decrease of the temperature or an increase of the salt concentration, but also to the increase in volume fraction.[24,25] The latter point could be explained by the increase in counterion concentration, which has a major effect in screening ionic repulsions, as explained above. This screening of ionic repulsions may cause an increase in the size of the equilibrium cluster, until the repulsions are so low that a barrier no longer exists for lysozyme self-association.

At this point the association of lysozyme into equilibrium clusters is preempted by crystallization.

The fitted model still fails to describe quantitatively the strength of ionic repulsions at low ionic strength, and also the strength of attractions at high ionic strength.

The discrepancy between the experimental data and the model could be due to the simplicity of the assumptions of our model (uniformly charged spherical particles). It could also be due to specific interactions of salt ions with protein residues, which are the subject of a very active debate.[46–50] In particular, deviations of the effective net charge from the predicted one may be caused by added salt due not only to ionic strength effects but also to specific ion effects.[51–53]

5 Conclusion

Our results show complete experimental osmotic pressures *vs.* volume fraction for the aqueous solutions of a protein. Each point of these curves illustrates an equilibrium state of the lysozyme solution. Relationships between the osmotic pressure and the concentration in solutions of lysozyme and a few other proteins have already been described,[11–14,20,54,55] but our experiments span much wider ranges of osmotic pressures and concentrations. As a consequence, all the states classically described for protein solutions have been explored, from the ideally dilute solution to the solid state, for which the solidus line, usually extrapolated from the density of crystals, is poorly described in phase diagrams.[56] Moreover, these data highlight the crystallization transition, and its displacement towards lower volume fractions caused by the decrease of the range and the strength of electrostatic interactions. The crystallization transition shown by our data is consistent with the solubility data available in the literature,[44] and with a crystal space group well known for lysozyme.[45]

Simple colloidal models, without interactions other than steric, such as the Carnahan–Starling model, do not reproduce any of our data series. However, for all our experimental data, the low packing fraction region up to the crystallization event is correctly described by the combination of a steric repulsion (Carnahan–Starling model), van der Waals forces and a screened electrostatic repulsion as described by the classical Debye–Hückel potential, provided that the contribution from the counterions of the proteins to the screening is taken into account. Quantitative agreement between this model and the experimental data would probably require to take into account the shape and charge distribution of the molecules. The possible specific interactions between ions and protein residues[51,57–59] could also make the electrical charge of the protein deviate from theoretical predictions based of the pK_a of the amino acids.

The mechanisms involved in our description of the dilute part of the osmotic pressure *vs.* volume fraction of lysozyme, *i.e.* the balance between short-range attraction and long-range repulsion, have been described for colloids[60] and lysozyme[24] and may be applicable to other proteins. However, some features of our experimental data are related to specific properties of lysozyme, like its ability to crystallize under the physicochemical conditions we used. Indeed, the plateau reflecting the crystallization transition has not yet been observed for other globular proteins, such as ovalbumin[12] or BSA.[11] This may be due to the smaller range of concentrations, but more likely to the experimental conditions (pH, ionic strength, nature of salts, kinetics of concentration, temperature) that, depending on the protein, favor behaviors other than crystallization when the solutions are highly concentrated. The high concentration part of the osmotic pressure *vs.* volume fraction curve is then probably also controlled by other protein properties, such as the anisotropy of the shape and charge density. The determination of the contribution of these structural specificities in the equations of state of proteins is still to be explored.

Acknowledgements

The authors thank Martine Meireles, Yannick Hallez, Christophe Labbez, Marie Skepö, Valérie Briard-Bion, and Julien Jardin for helpful discussions.

References

1 A. D. Marshall, P. A. Munro and G. Trägårdh, *Desalination*, 1993, **91**, 65–108.
2 M. E. M. Cromwell, E. Hilario and F. Jacobson, *AAPS J.*, 2006, **8**, E572–E579.
3 P. Ball, *Nat. Mater.*, 2012, **11**, 185.
4 A. U. Borwankar, A. K. Dinin, J. R. Laber, A. Twu, B. K. Wilson, J. A. Maynard, T. M. Truskett and K. P. Johnston, *Soft Matter*, 2013, **9**, 1766.
5 K. P. Johnston, J. A. Maynard, T. M. Truskett, A. U. Borwankar, M. A. Miller, B. K. Wilson, A. K. Dinin, T. A. Khan and K. J. Kaczorowski, *ACS Nano*, 2012, **6**, 1357–1369.
6 R. J. Ellis and A. P. Minton, *Nature*, 2003, **425**, 27–28.
7 A. Saluja and D. S. Kalonia, *Int. J. Pharm.*, 2008, **358**, 1–15.
8 F. Carlsson, M. Malmsten and P. Linse, *J. Phys. Chem. B*, 2001, **105**, 12189–12195.
9 F. Cardinaux, E. Zaccarelli, A. Stradner, S. Bucciarelli, B. Farago, S. U. Egelhaaf, F. Sciortino and P. Schurtenberger, *J. Phys. Chem. B*, 2011, **115**, 7227–7237.
10 C. Gögelein, G. Nägele, R. Tuinier, T. Gibaud, A. Stradner and P. Schurtenberger, *J. Chem. Phys.*, 2008, **129**, 085102.
11 V. L. Vilker, C. K. Colton and K. A. Smith, *J. Colloid Interface Sci.*, 1981, **79**, 548–566.
12 M. A. Yousef, R. Datta and V. G. J. Rodgers, *J. Colloid Interface Sci.*, 2001, **243**, 321–325.
13 Y. U. Moon, C. O. Anderson, H. W. Blanch and J. M. Prausnitz, *Fluid Phase Equilib.*, 2000, **168**, 229–239.
14 Y. U. Moon, R. A. Curtis, C. O. Anderson, H. W. Blanch and J. M. Prausnitz, *J. Solution Chem.*, 2000, **29**, 699–718.
15 C. Bonnet-Gonnet, L. Belloni and B. Cabane, *Langmuir*, 1994, **10**, 4012–4021.
16 A. S. Robbes, F. Cousin and G. Meriguet, *Braz. J. Phys.*, 2009, **39**, 156–162.

17 C. Martin, F. Pignon, A. Magnin, M. Meireles, V. Lelièvre, P. Lindner and B. Cabane, *Langmuir*, 2006, **22**, 4065–4075.
18 A. Mourchid, A. Delville, J. Lambard, E. Lécolier and P. Levitz, *Langmuir*, 1995, **11**, 1942–1950.
19 C. Vauthier, B. Cabane and D. Labarre, *Eur. J. Pharm. Biopharm.*, 2008, **69**, 466–475.
20 A. Bouchoux, G. Gésan-Guiziou, J. Pérez and B. Cabane, *Biophys. J.*, 2010, **99**, 3754–3762.
21 A. Bouchoux, P.-E. Cayemitte, J. Jardin, G. Gésan-Guiziou and B. Cabane, *Biophys. J.*, 2009, **96**, 693–706.
22 R. Parker, T. R. Noel, G. J. Brownsey, K. Laos and S. G. Ring, *Biophys. J.*, 2005, **89**, 1227–1236.
23 G. J. Brownsey, T. R. Noel, R. Parker and S. G. Ring, *Biophys. J.*, 2003, **85**, 3943–3950.
24 A. Stradner, H. Sedgwick, F. Cardinaux, W. C. K. Poon, S. U. Egelhaaf and P. Schurtenberger, *Nature*, 2004, **432**, 492–495.
25 A. Stradner, F. Cardinaux and P. Schurtenberger, *J. Phys. Chem. B*, 2006, **110**, 21222–21231.
26 A. Shukla, E. Mylonas, E. D. Cola, S. Finet, P. Timmins, T. Narayanan and D. I. Svergun, *Proc. Natl. Acad. Sci. U. S. A.*, 2008, **105**, 5075–5080.
27 P. Kowalczyk, A. Ciach, P. Gauden and A. Terzyk, *J. Colloid Interface Sci.*, 2011, **363**, 579–584.
28 Y. Liu, L. Porcar, J. Chen, W.-R. Chen, P. Falus, A. Faraone, E. Fratini, K. Hong and P. Baglioni, *J. Phys. Chem. B*, 2011, **115**, 7238–7247.
29 D. L. Rickard, P. B. Duncan and D. Needham, *Biophys. J.*, 2010, **98**, 1075–1084.
30 O. D. Velev, E. W. Kaler and A. M. Lenhoff, *Biophys. J.*, 1998, **75**, 2682–2697.
31 A. C. Dumetz, A. M. Chockla, E. W. Kaler and A. M. Lenhoff, *Biophys. J.*, 2008, **94**, 570–583.
32 D. F. Rosenbaum and C. F. Zukoski, *J. Cryst. Growth*, 1996, **169**, 752–758.
33 E. J. Park and Y. C. Bae, *Biophys. Chem.*, 2004, **109**, 169–188.
34 S. P. Rozhkov and A. S. Goryunov, *Biophys. Chem.*, 2012, **170**, 34–41.
35 M. Muschol and F. Rosenberger, *J. Chem. Phys.*, 1997, **107**, 1953.
36 J. Wang, M. Dauter, R. Alkire, A. Joachimiak and Z. Dauter, *Acta Crystallogr., Sect. D: Biol. Crystallogr.*, 2007, **63**, 1254–1268.
37 H. Li, A. D. Robertson and J. H. Jensen, *Proteins: Struct., Funct., Bioinf.*, 2005, **61**, 704–721.
38 M. H. M. Olsson, C. R. Søndergaard, M. Rostkowski and J. H. Jensen, *J. Chem. Theory Comput.*, 2011, **7**, 525–537.
39 J. A. Cohen, R. Podgornik, P. L. Hansen and V. A. Parsegian, *J. Phys. Chem. B*, 2009, **113**, 3709–3714.
40 V. A. Sirotkin, I. A. Komissarov and A. V. Khadiullina, *J. Phys. Chem. B*, 2012, **116**, 4098–4105.
41 N. F. Carnahan and K. E. Starling, *J. Chem. Phys.*, 1969, **51**, 635–636.
42 A. Humeny, T. Kislinger, C.-M. Becker and M. Pischetsrieder, *J. Agric. Food Chem.*, 2002, **50**, 2153–2160.
43 P. Richard, L. Oger, J.-P. Troadec and A. Gervois, *Phys. Rev. E: Stat. Phys., Plasmas, Fluids, Relat. Interdiscip. Top.*, 1999, **60**, 4551–4558.
44 P. Retailleau, M. Riès-Kautt and A. Ducruix, *Biophys. J.*, 1997, **73**, 2156–2163.
45 K. P. Wilson, B. A. Malcolm and B. W. Matthews, *J. Biol. Chem.*, 1992, **267**, 10842–10849.
46 P. Jungwirth, *J. Phys. Chem. Lett.*, 2013, **4**, 4258–4259.
47 K. B. Rembert, J. Paterová, J. Heyda, C. Hilty, P. Jungwirth and P. S. Cremer, *J. Am. Chem. Soc.*, 2012, **134**, 10039–10046.
48 J. Paterová, K. B. Rembert, J. Heyda, Y. Kurra, H. I. Okur, W. R. Liu, C. Hilty, P. S. Cremer and P. Jungwirth, *J. Phys. Chem. B*, 2013, **117**, 8150–8158.
49 H. I. Okur, J. Kherb and P. S. Cremer, *J. Am. Chem. Soc.*, 2013, **135**, 5062–5067.
50 W. J. Xie and Y. Q. Gao, *J. Phys. Chem. Lett.*, 2013, **4**, 4247–4252.
51 A. Kurut and M. Lund, *Faraday Discuss.*, 2013, **160**, 271–278.
52 M. Boström, D. R. M. Williams and B. W. Ninham, *Biophys. J.*, 2003, **85**, 686–694.
53 C. A. Haynes, E. Sliwinsky and W. Norde, *J. Colloid Interface Sci.*, 1994, **164**, 394–409.
54 C. A. Haynes, K. Tamura, H. R. Korfer, H. W. Blanch and J. M. Prausnitz, *J. Phys. Chem.*, 1992, **96**, 905–912.
55 D. Farrer and A. Lips, *Int. Dairy J.*, 1999, **9**, 281–286.
56 P. G. Vekilov, *Soft Matter*, 2010, **6**, 5254–5272.
57 M. Boström, F. W. Tavares, S. Finet, F. Skouri-Panet, A. Tardieu and B. W. Ninham, *Biophys. Chem.*, 2005, **117**, 217–224.
58 Y. Zhang and P. S. Cremer, *Proc. Natl. Acad. Sci. U. S. A.*, 2009, **106**, 15249–15253.
59 J. Zhang, in *Protein-Protein Interactions – Computational and Experimental Tools*, ed. W. Cai, InTech, 2012, pp. 359–376.
60 J. Groenewold and W. K. Kegel, *J. Phys. Chem. B*, 2001, **105**, 11702–11709.